Proceedings of the ASME 2022
International Mechanical Engineering Congress and Exposition
IMECE2022
October 30-November 3, 2022, Columbus, Ohio

IMECE2022-94931

NUMERICAL INVESTIGATION OF ULTRASONIC PHASED ARRAY REVERSE TIME MIGRATION TECHNIQUE CONSIDERING SPATIAL WAVE CHARACTERISTICS

Shulong Zhou
University of Michigan-Shanghai Jiao Tong University Joint Institute, Shanghai Jiao Tong University, Shanghai, China

Yanfeng Shen
University of Michigan-Shanghai Jiao Tong University Joint Institute, Shanghai Jiao Tong University, Shanghai, China;
Shanghai Key Laboratory for Digital Maintenance of Buildings and Infrastructure, Shanghai, China

ABSTRACT

This paper presents a systematic numerical research on ultrasonic phased array reverse time migration technique for damage evaluation in bulk materials. In this study, a thick aluminum bulk is used as the target structure to be tested, and an ultrasonic phased array composed of piezoelectric elements and damping blocks is prosed as the transducers for generating and receiving elastic waves. Firstly, a Finite Element Model (FEM) of a pair of transducers is established to study the wave generation and reception performance. In particular, the suppression effect of different backing material parameters (damping ratio, thickness, implementation details) on the piezo-elements to absorb excessive resonant vibrations is investigated, in order to send out and receive spatially squeezed mechanical pulses into the target medium. Then, a full-scale FEM is established with the complete probe set and typical structural damage types to understand the wave propagation and its interaction with damage. Both longitudinal (L) and shear (S) waves are studied, while they interact with a hole and cracks with different orientations with respect to the incident wave direction. Finally, the reverse time migration algorithm is further developed by considering the spatial wave characteristics. The amplitude variation along the propagation distance is taken into account to form a time/space-gain compensation function to improve the damage imaging quality and sensitivity, especially for far field damage sites. At the same time, the imaging algorithm is tested for the single L-wave, the single S-wave, and the fused LS-wave scenarios. It was found that the combination of L-mode and S-mode can significantly improve the damage imaging results. This numerical investigation may lay a solid foundation for the development of ultrasonic phased array technique for non-destructive evaluation (NDE) of bulky materials. This paper ends with a summary, concluding remarks, and suggestions for future work.

Keywords: nondestructive evaluation; damage detection; ultrasound; phased array; reverse time migration

1. INTRODUCTION

Ultrasonic phased array technology has been extensively investigated by academia and industry as a powerful approach for non-destructive evaluation purpose. The development of novel ultrasonic phased array probes and high-quality imaging algorithms forms the key directions of scientific research advancement in this regard.

The advent of ultrasonic ring dynamic focusing probe developed by TOMB marked the emergence of ultrasonic phased array technology[1]. Kino put forward the aperture focusing theory which laid a theoretical foundation for the development of ultrasonic imaging method[2]. Devos developed a two-dimensional matrix semi-flexible phased array probe whose detection rate, reliability and detection efficiency improved accordingly compared with the traditional one-dimensional linear array probes[3]. Subsequently, Walter and Wong successfully achieved a new ultrasonic phased array probe adopting PMN-PT (ferroelectric single crystal) composite material, which showed higher sensitivity and wider frequency band range compared with PZT (lead zirconate carbonate) phased array probes[4, 5]. At the same time, there exist a series of researches on the simulation of ultrasonic probes. Liu utilized the commercial finite element code ANSYS to simulate the ultrasonic wave propagation, which showed the computation featuring the wave propagation process and wavefield characteristics[6]. Gao determined the shape of the damage utilizing the spectrum of the damage-echo signals obtained by

FEM simulation[7]. Numerical modeling of ultrasonic phased array can provide a theoretical basis for the design and manufacture of ultrasonic phased array probes. Numerical investigations can facilitate an in-depth understanding of the mechanism behind the complex waves phenomena excited by ultrasonic phased array and the formulation of the imaging algorithms. However, such numerical study and simulation results are still very limited and should be further extended.

Reverse-time Migration (RTM) technique was originally developed in geophysics[1, 8, 9] and had been introduced to elastic wave-based damage imaging with good imaging performance[10-14]. RTM involves the time reversal operation focusing method and performs the back-propagation process in data post-processing. Extrapolating the time-reversed scattered wavefields using numerical methods such as finite difference algorithms focuses wave energy toward damaged regions[10, 15]. The time-reversed backscattered signals would focus towards the source location, even if the objects are of complex shapes. The self-focusing process could also be used in plate-like structures[16]. An excitation-time imaging condition, which used only the center frequency of the excitation signal, was employed by Lin and Yuan[10]. Zhu et al. employed RTM in the frequency domain[11]. Rodriguez et al. applied similar principles using a linear array with 128 elements to excite plane waves normal to the boundary of an isotropic plate[12]. He and Yuan employed a zero-lag cross-correlation (ZLCC) algorithm as an imaging condition, which utilized all the input frequencies and the dispersion effect was compensated automatically during the back propagation of the time-reversed scattered wave signals[13]. To date, ultrasonic phased arrays were used in conjunction with RTM for seismic exploration, NDE of bulk materials, and damage imaging in thin plates. Although many new advancements are being achieved to realize better damage assessment, further investigations on the imaging algorithm improvements are still desired and stay as the key topic for phased array techniques.

This paper presents a systematic numerical investigation of the ultrasonic phased array technique for NDE of bulk materials. The suppression effect of different backing layer material parameters on the wave pulse generated by piezo-elements is investigated to eliminate the interference waves and obtain the high-frequency, spatially squeezed longitudinal and shear waves for damage imaging. The longitudinal and shear waves generation, propagation, and their interaction with a hole and cracks with different orientations with respect to the incident wave direction on bulk materials will be showcased. Damage detection based on reverse time migration technology are presented to demonstrate the superb capability of the ultrasonic phased array for non-destructive evaluation on bulky materials.

2. NUMERICAL INVESTIGATION ON THE BACKING MATERIAL FOR TRANSDUCER RESONANCE SUPPRESSION

In this section, Multi-group coupled-filed transient dynamic finite element models were demonstrated. Utilizing those models, both different damping ratio and different thickness of backing layer materials were considered to illustrate the effect of different backing layer material parameters on absorbing excessive resonant vibrations for selecting the reasonable material parameters.

FIGURE 1 presents the 2D transient dynamic coupled-field finite element model. The model simulated an aluminum bulk material with a pair of transducers and a backing material layer in the top over the transducers. The width of aluminum material was 50 mm and the thickness was 80 mm. It should be noted that only the influence of the backing material parameters was investigated in this section. These two piezo elements were used for ultrasonic wave generation and reception, respectively. The epoxy material served as the backing layer, which can effectively damp the ringing effects (excessive vibrations) of the piezoelectric elements, shortening the spatial pulse length and broadened the band width, so as to improve the image axial resolution. In addition, the surrounding epoxy filler effectively strengthen the transverse vibration reaction forced at the PZT pillars, leading to enhanced longitudinal waves that propagate into the target objects.

In ultrasonic imaging technologies, increasing the transmission frequency can improve the resolution nevertheless the attenuation of the excitation signal in the specimen increases. Choosing the appropriate frequency is the fundamental step to ensure the resolution of the reconstructed image. The first derivative of Blackman Harris (BHW wavelet) was usually used as the excitation waveform in most practices[17]. In this paper the pulse wave was selected in light of the industrial requirements, with the waveform shown in FIGURE 2. Non-reflective Boundaries (NRB) were implemented at the bottom and two sides of the aluminum bulk. The coverage of NRB extended over 40 mm, which could guarantee the effective absorption of boundary reflections. To solve the problem accurately and efficiently, the mesh size and time step were optimized. The element size was set to 0.1 mm, which could guarantee enough points to depict up to the high frequency spatial wavelength at 3.2 MHz and the time step was set to 0.01μs, which can also satisfy the accuracy requirement of the temporal period.

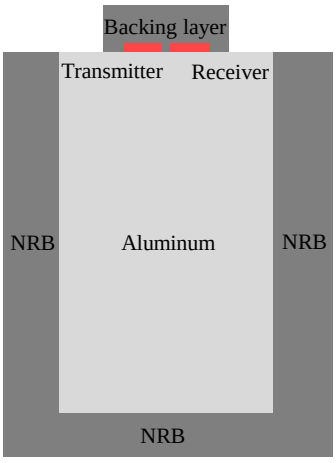

FIGURE 1: FULL-SCALE FINITE ELEMENT MODEL

2.1 Absorbing effect of excessive vibration by backing materials with different thicknesses

Six groups of simulations were carried out for exploring the absorption effect of backing materials on excessive vibration with different thicknesses. To better illustrate the suppression effect of the backing materials, a comparative model was also constructed with only a pair of transducers in the top of the specimen, but without the backing materials. Other aspects of the comparative model were kept the same as the backing material model. FIGURE 3 presents the simulation results for the suppression effect of backing materials. The amplitude of the sensing signal attenuates to a certain extent, nevertheless the excessive vibration can be suppressed more quickly with the increase of the thickness of the backing material. In contrast, there existed obvious trembling coda waves due to the excessive vibration in the comparative case. Combining the practical industrial demand and the simulation results, a 10-mm thick backing material layer was finally selected for the follow-up numerical simulations.

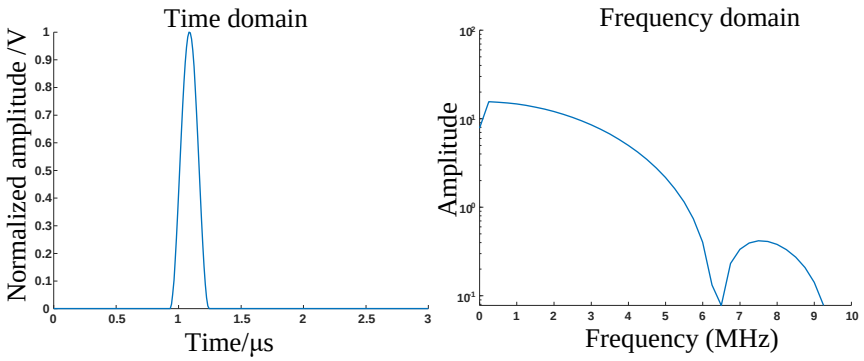

FIGURE 2: EXCITING SIGNAL FOR THE NUMERIAL INVESTIGATIONS: (A) TIME DOMIAN OF EXCITING SIGNALS; (B) FREQUENCY DOMIAN OF EXCITING SIGNALS

2.2 Absorbing effect of excessive vibration by backing materials with various damping ratios

Another factor affecting the backing materials to suppress the excessive vibration is their damping ratios. Based on the previous simulation results, seven groups of case studies were carried out to sort the ideal damping ratio of the backing material. FIGURE 4 presents the simulation results for the suppression effect of backing materials. The coda waves of the sensing signals for various backing material damping ratio cases were shown. It is apparent that the backing material with a damping ratio of 0.02 performed very well for resonance attenuation.

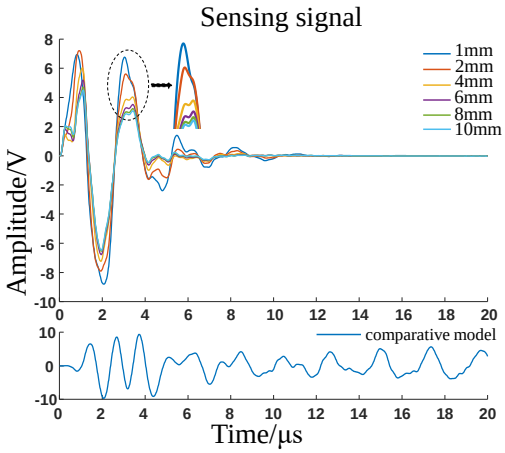

FIGURE 3: RESONANCE ABSORBING PERFROMANCE ASSICATED WITH BACKING MATERIAL THICKNESS

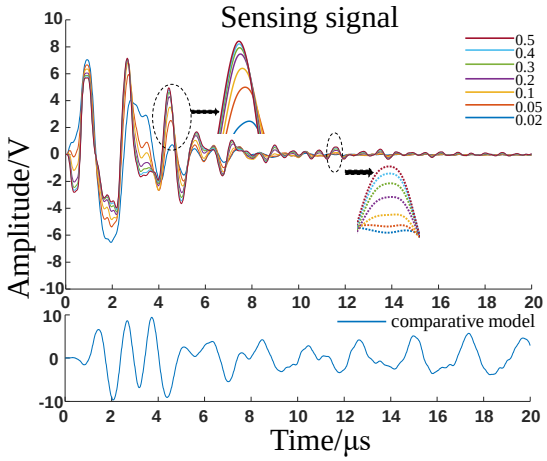

FIGURE 4: RESONANCE AOBSROBING PERFORAMANCE ASSOCIATED WITH BACKING MATERIAL DAMPING RATIO

3. SIMULATION OF WAVE INTERACTION WITH TYPICAL STRUCTURAL DAMAGE TYPES

After investigating the resonance suppression performance of the backing material, numerical case studies on wave propagation and interaction with various types of damage were conducted. The overall configurations of FEM model considered a 100-mm wide, 50-mm thick aluminum bulk, as shown in FIGURE 5. The damping ratio of the backing material was 0.02 and the thickness was 10 mm. A hole and cracks with different orientations with respect to the incident wave direction were examined at the position 80 mm below the. A comparative

pristine case was also investigated. The diameter of the hole was 5mm and the length of the cracks also took 5mm. The pulse wave was loaded on the transmitter to generate the ultrasonic waves.

FIGURE 6 shows the snapshots of the stress wave field as well as the representative sensing signals from different models. Effective wave absorption at the Non-reflective boundaries can be noticed. In the damage cases, scattered waves from the damage sites can be clearly identified. Longitudinal wave was present in the beginning and shear wave followed during wave propagation. Behind the shear waves, electromechanical resonances causing subtle sequential waves were observed as a result of the resonating coupling effect at the piezo transducers. The second red circled lines illustrated the reflections from damage sites in FIGURE 6a, which also presented the resonant signal had no interference on the subsequent reflected waves.

Different types of damage have distinctive effects on wave scattering. The signal was reflected and diffused in a circular wavefront when the longitudinal wave interacted with the hole damage, while the reflected waves showed strong directivity with respect to the crack trace orientation due to different impinging angles. It is worth noting that the scattered wave propagated at a certain angle along both sides of the crack and continued to propagate along the original propagation direction when the longitudinal wave interacted with a vertical crack as presented in FIGURE 6d. The oblique wave incident angle and strong directivity of wave scattering made it a great difficulty to acquire a high-amplitude reflected signals at the sensory terminals.

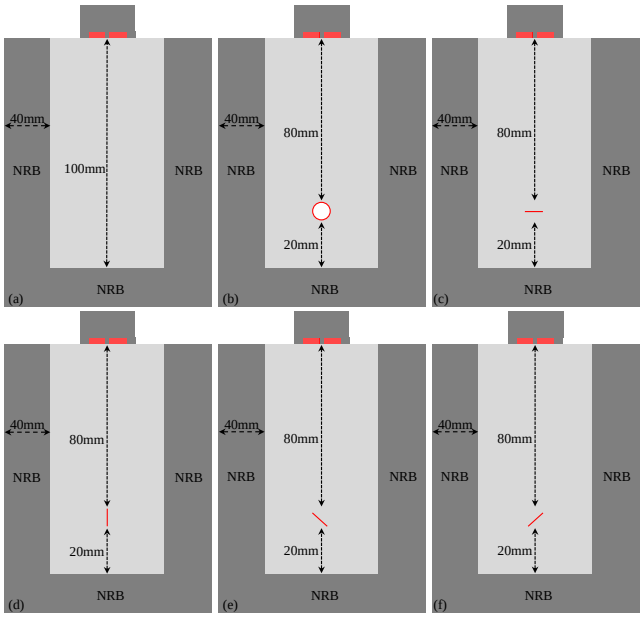

FIGURE 5: FINITE ELEMENT MODEL LAYOUT FOR WAVE INTERACTION WITH DIFFERENT DAMAGE SCIENARIOS: (A) PRISTINE CASE; (B) A HOLE; (C) A HORIZONGTAL CRACK; (D) A VERTICAL CRACK; (E) A RIGHT OBLIQUE CRACK; (F) A LEFT OBLIQUE CRACK

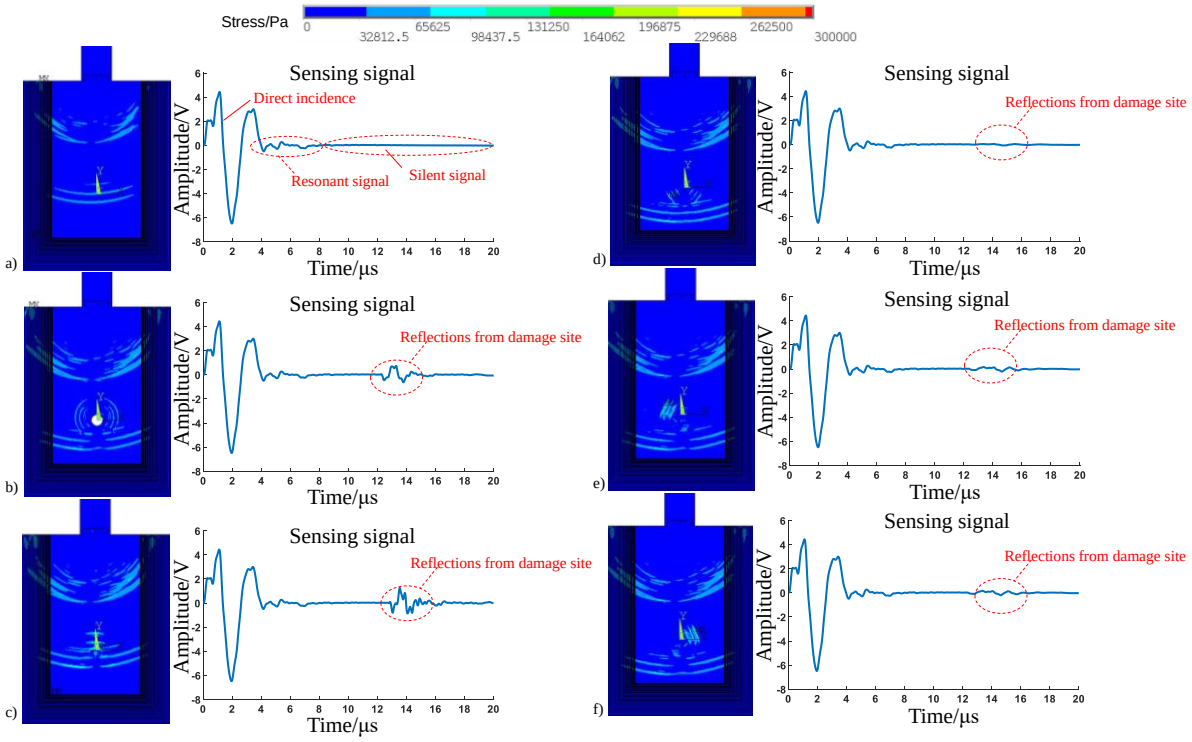

FIGURE 6: THE WAVE PROPAGATION SNAPSHOTS AND THE SENSING SIGNALS IN THE ALUMINUM SPECIMEN: (A) THE PRISTINE MODEL; (B) A HOLE CASE; (C) A HORIZONTAL CRACK CASE; (D) A VIRTICAL CRACK CASE; (E) A RIGHT OBLIQUE CRACK CASER; (F) A LEFT OBLIQUE CRACK CASE

4. THE REVERSE TIME MIGRATION FOR DAMAGE IMAGING

In order to achieve high-quality structural sensing, damage localization and imaging techniques are employed, among which reverse time migration method has been extensively investigated and developed towards its mature stage. Thus, the reverse time migration algorithm is used to construct active sensing images. The proposed technique for damage identification consists of three steps: obtaining the forward-time extrapolation from the source, reversing the time extrapolating of the received wave field, and finally applying a focusing condition for imaging the damage. The forward-time extrapolation was carried out and the received scattered wave signals were obtained at sensor locations through simulation of structures with damage using finite elements. The overall configurations of the FEM model were displayed as a 100-mm wide, 60-mm thick aluminum bulk in FIGURE 7. The Non-Reflective Boundaries were increased to 60-mm thick for eliminating the influence of boundary reflection completely and the 5mm-diameter holes were simulated as the damage.

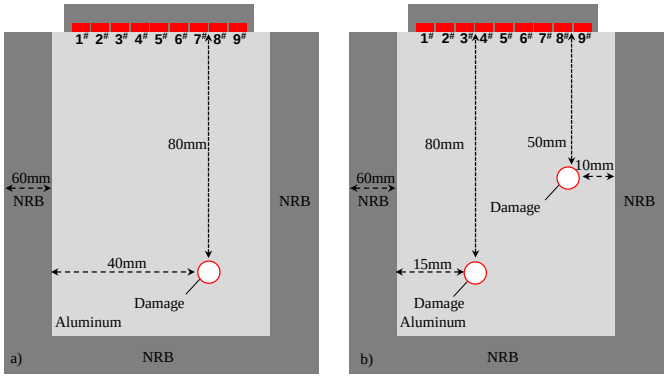

FIGURE 7: FINITE ELEMENT MODEL FOR PHASED ARRAY ACTIVE SENSING: A) ONE-DAMAGE-LOCATION CASE; B) TWO-DAMAGE-LOCATION CASE

During each round of simulation, one piezo element would serve as the transmitter and the remaining ones would work as receivers to sense the reflected signal from the damage. FIGURE 8a presents the sensing signals from the remaining eight piezoelectric discs functioning as sensors and the piezo element #1 functioned as the transmitter. From the time domain signals, many wavy forms can be observed which represents the reflected signals consisting of the L-wave captured from the interaction between the damage and longitudinal waves as well as the S-wave captured from wave mode conversion. The sensing signals present complexity and superposition in the two-damage case compared with the one-damage case. Due to the difference in the position of the damage sites and the difference in the propagation velocity of waves, the scattered waves were superimposed to a certain extent, which made the subsequent analysis and processing of the signal difficult and cumbersome, such as the superposition of L-wave and S-wave in FIGURE 8d.

The modeling work assumed a 2-D damage geometry, indicating that the damage was infinite in the third dimension. The scattering matrix, S, described the amplitude of the scattered wave that would be measured if the distance from defect to receiver was normalized to one wavelength. When a plane wave of amplitude u_0 incidents on a defect, the scattered field decays (in the far field) in inverse proportion to the square root of the distance from the defect. Hence, the amplitude of the scattered wave, u_s, at a distance r_2 (where r_2 is in the far-field of the defect) from a defect is given by[18]:

$$u_s = u_0 S(\theta_1, \theta_2)\sqrt{\frac{\lambda}{r_2}}e^{ik(r_2-\lambda)} \quad (1)$$

where λ is the wavelength of the ultrasonic wave, k is wavenumber (k = 2π/λ), θ_1 is the incident wave angle, and θ_2 is the scattering direction. In this paper, the displacement magnitudes were multiplied by $\sqrt{1/r}$ and divided by the averaged magnitude as the compensation fact.

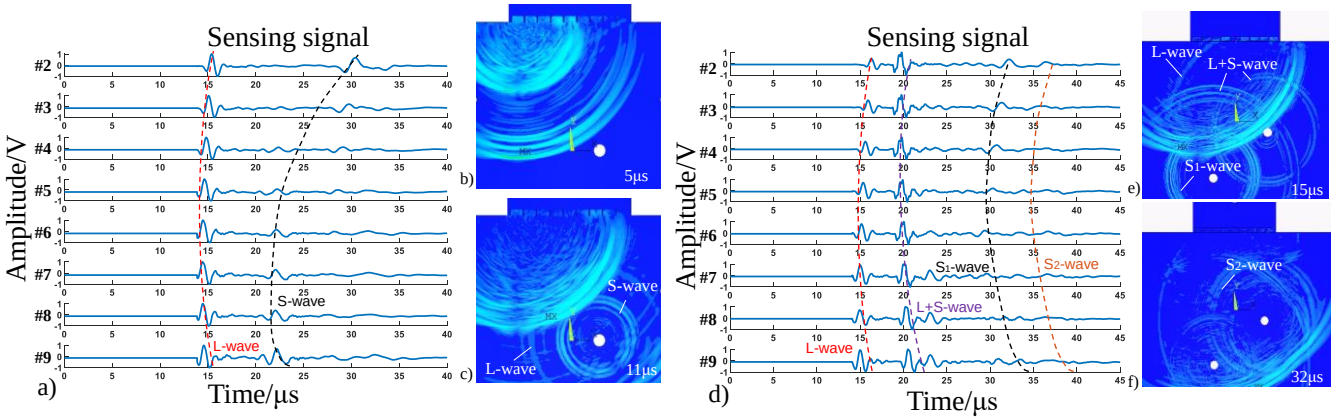

FIGURE 8: SENSING SIGNALS AND WAVEFIELD IMAGES WITH PZT #1 AS THE TRANSMITTER: A) SENSING SIGNALS FROM ONE-DAMAGE-LOCATION CASE; B) THE WAVE PROPAGATION SNAPSHOTS AT 5 MICROSECONDS; C) THE WAVE PROPAGATION SNAPSHOTS AT 11 MICROSECONDS; D) SENSING SIGNALS FROM TWO-DAMAGE-LOCATION CASE; E) THE WAVE PROPAGATION SNAPSHOTS AT 5 MICROSECONDS; F) THE WAVE PROPAGATION SNAPSHOTS AT 32 MICROSECONDS

FIGURE 9 shows the modified sensing signals. The reflected waves were obviously improved after compensation in accordance with the amplitude attenuation, especially for the shear waves. The imaging accuracy was effectively improved by compensated sensing signal in FIGURE 11. The superposition of reflected waves was presented in FIGURE 9b.

Back-propagation of the time-reversed scattered signals at all sensor locations generate the backward wave field. The backward wave field will be converging back to damage sites. Scattering waves from damage are considered as a secondary wave source. The signals were further enveloped to represent the wave packet energy propagation and focusing phenomena. These signals processing procedure is presented in FIGURE 10.

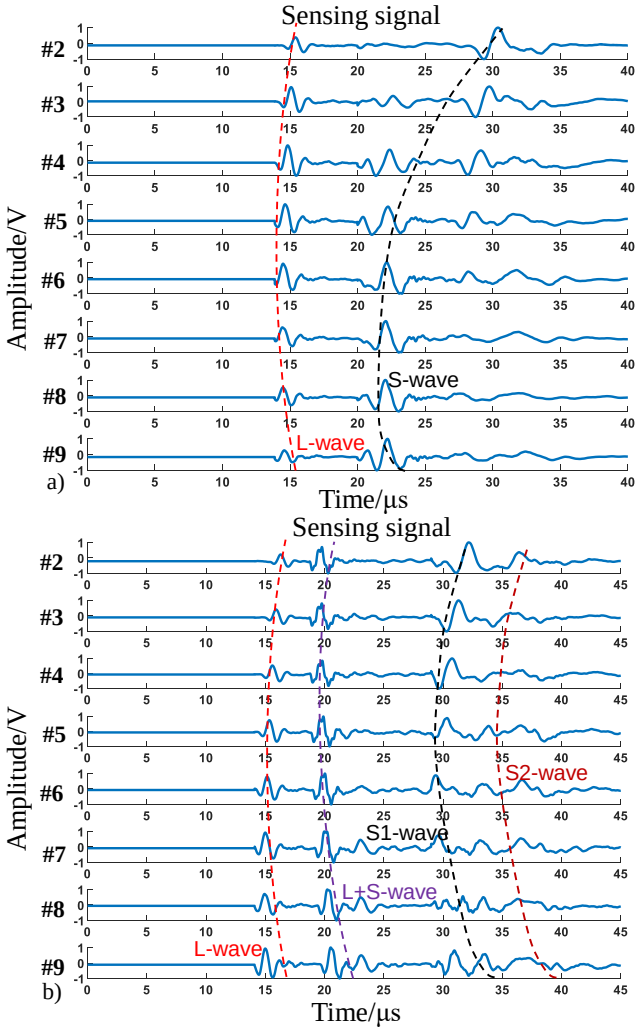

FIGURE 9: COMPENSATED SENSING SIGNALS COLLECTED WITH PIEZO ELEMENT #1 AS THE TRANSMITTER: A) ONE-DAMAGE-LOCATION CASE; B) TWO-DAMAGE-LOCATION CASE

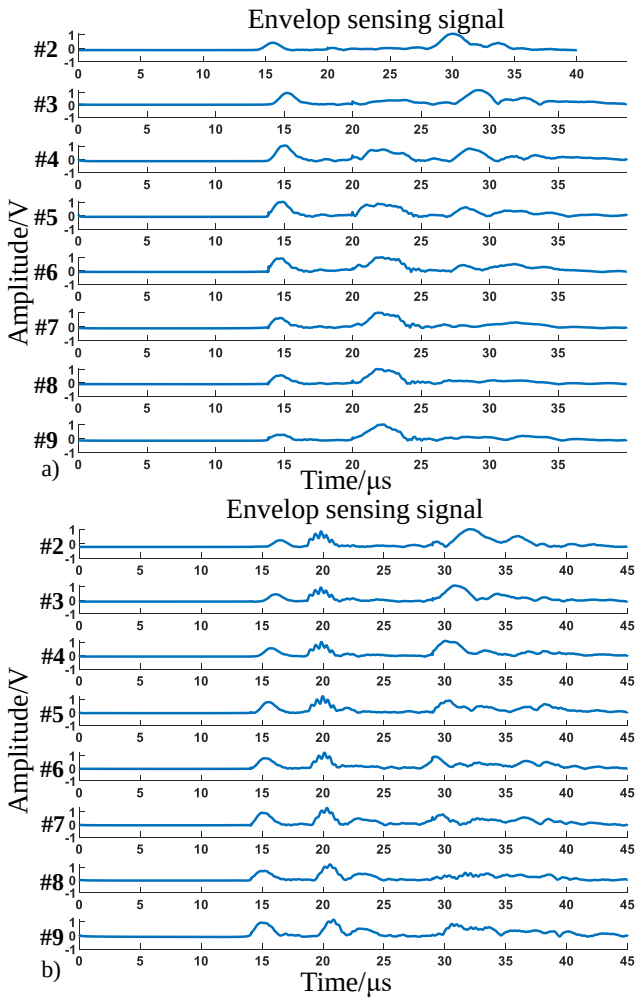

FIGURE 10: SIGNALS PROCESSED WITH ENVELOPE CURVES: A) ONE-DAMAGE-LOCATION CASE; B) TWO-DAMAGE-LOCATION CASE

The imaging algorithm can be expressed as

$$S(i,j) = \prod_{m=1}^{N} A_m V_m(t_{mij}) \quad (2)$$

$$t_{mij} = [R_m^a(i,j) + R_m^s(i,j)]/cg \quad (3)$$

where A_m is the unifying weighting function; $V_m(t_{mij})$ represents the time domain sensing signal after the enveloping procedure; t_{mij} stands for the time elapse of wave propagation from the actuator to the pixel location (i,j) and back to the sensor; the subscript m represents the sensing pair m; N represents the maximum number of sensing pairs; R_m^a and R_m^s are the distances from the actuator to the pixel location and from the pixel location to the sensor, respectively; $c\_g = 6.3$ km/s is the velocity of the longitudinal wave and $c\_g = 3.3$ km/s is the velocity of the shear wave.

FIGURE 11 shows the damage imaging comparison results before and after the spatial function compensation. The red circles illustrate the location of the damage. Before the compensation, the damage sites cannot be imaged accurately via

the L and S wave fused information with a point-to-point pixel multiplication algorithm, especially for the two-damage-location case. The paths crossing the damage sites were highlighted. On the other hand, the damage imaging quality was apparently improved after the fused LS-wave scenarios. There were obviously two high-pixel areas in the modified LS-wave imaging results, clearly representing the two damage sites.

Although the imaged damage positions deviated a little bit from the true damage sites, it had been obviously improved using the pixel multiplication algorithm with spatial wave amplitude compensation. The damage sites can be accurately located via the high image pixel values for both near field and far field locations.

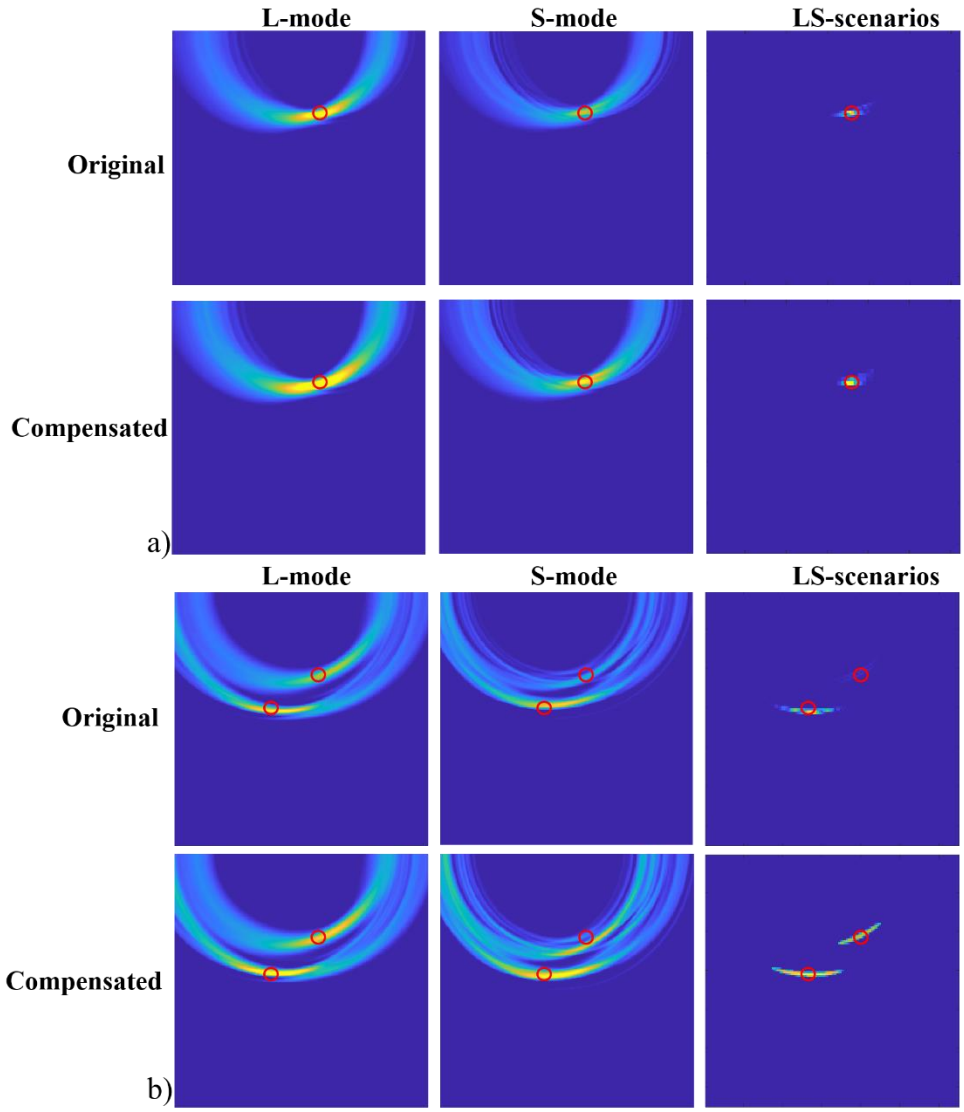

FIGURE 11: DAMAGE IMAGING BEFORE AND AFTER COMPENSATION: (A) ONE-DAMAGE-LOCATION CASE; (B) TWO-DAMAGE-LOCATION CASE

5. CONCLUDING REMARKS AND FUTURE WORK

This paper presented a systematic numerical investigation on ultrasonic phased array reverse time migration technique for damage detection in bulk materials. This research explored the backing material parameters and found that these parameters imposed great influence on suppressing the transducer resonances. It was found that appropriate thickness and damping ratio for the backing material can lead to absorbing excessive resonant vibration, which may contribute to a cleaner sensing signal. Then, comparative FEM simulations were conducted. The generation and propagation of L-wave and S-wave in bulk materials and their interaction with a hole and cracks with different orientations were studied. It was concluded that the signal scattered and diffused as a circle when the longitudinal wave interacted with the hole damage, while the scattered waves showed intensive directivity associated with the impinging

angles with respect to the crack traces. Furthermore, damage detection based on inverse time migration technology was presented to demonstrate the superb capability of the ultrasonic phased array for non-destructive evaluation of bulky materials. It was found that the LS-wave fused imaging algorithm with spatial compensation can substantially improve the image the structural damage.

For work, the proposed phased array probe and imaging algorithm should be implemented in experimental setups for performance validation and industrial applications.

REFERENCES

[1] E. Baysal, D. Kosloff, and J. Sherwood, "Reverse-Time Migration," *Geophysics,* vol. 48, pp. 1514-1524, 1983.

[2] B. W. Drinkwater and P. D. Wilcox, "Ultrasonic arrays for non-destructive evaluation: A review," *NDT & E International,* vol. 39, no. 7, pp. 525-541, 2006.

[3] D. Devos, G. Maes, and P. Tremblay, "Optimized Semi-Flexible Matrix Array Probes for Large Rotor Shafts and DGS Sizing Diagram Simulation Tool," 2016.

[4] C.-M. Wong, Y. Chen, H. Luo, J. Dai, K.-H. Lam, and H. L.-w. Chan, "Development of a 20-MHz wide-bandwidth PMN-PT single crystal phased-array ultrasound transducer," *Ultrasonics,* vol. 73, pp. 181-186, 2017.

[5] S. Walter, T. Herzog, F. Schubert, and H. Heuer, "Comparison of Ultrasonic Phased Array Probes Based on PMN-PT and PZT 1-3 Composites," in *19th WCNDT World Conference on Non-Destructive Testing*, 2016.

[6] C. F. Liu, X. G. Niu, Z. W. Li, J. F. Zhao, S. Q. Jing, and G. W. Li, "Simulating Calculation of Propagations of Ultrasonic Longitudinal/Transverse Wave Based on ANSYS," 2011.

[7] J. Gao, Y. X. Chen, and Z. B. Wang, "Study of ultrasonic detection simulation for cylinders based on ANSYS," 2015.

[8] G. A. McMechan, "Migration by extrapolation of time-dependent boundary values*," *Geophysical Prospecting,* vol. 31, no. 3, pp. 413-420, 1983.

[9] S. A. Levin, "Principle of reverse‐time migration," *GEOPHYSICS,* vol. 49, no. 5, pp. 581-583, 1984.

[10] X. Lin and F.-G. Yuan, "Damage Detection of a Plate Using Migration Technique," *Journal of Intelligent Material Systems and Structures - J INTEL MAT SYST STRUCT,* vol. 12, 2001.

[11] R. Zhu, G. L. Huang, and F. G. Yuan, "Fast damage imaging using the time-reversal technique in the frequency–wavenumber domain," *Smart Materials and Structures,* vol. 22, no. 7, p. 075028, 2013.

[12] S. Rodriguez, M. Deschamps, M. Castaings, and E. Ducasse, "Guided wave topological imaging of isotropic plates," *Ultrasonics,* vol. 54, no. 7, pp. 1880-1890, 2014.

[13] J. He and F.-G. Yuan, "Damage identification for composite structures using a cross-correlation reverse-time migration technique," *Structural Health Monitoring,* vol. 14, no. 6, pp. 558-570, 2015.

[14] J. He and F.-G. Yuan, "An enhanced CCRTM (E-CCRTM) damage imaging technique using a 2D areal scan for composite plates," vol. 9804, 2016.

[15] I. F. Jones, "Tutorial: Migration imaging conditions," *First Break,* vol. 32, pp. 45-55, 2014.

[16] W. A. K. Deutsch, A. Cheng, and J. D. Achenbach, "Self-Focusing of Rayleigh Waves and Lamb Waves with a Linear Phased Array," *Research in Nondestructive Evaluation,* vol. 9, no. 2, pp. 81-95, 1997.

[17] H. Liu *et al.*, "Reverse time migration of acoustic waves for imaging based defects detection for concrete and CFST structures," *Mechanical Systems and Signal Processing,* vol. 117, pp. 210-220, 2019.

[18] L. W. Schmerr Jr., "Fundamentals of Ultrasonic Nondestructive Evaluation," *Springer,* vol. 122, no. 5, pp. 85-140, 2016.